J. Phys. B: At. Mol. Opt. Phys. 27 (1994) 4295–4308. Printed in the UK

Absolute elastic and inelastic electron scattering cross sections for xenon in the 15–100 eV impact-energy region

T Ester and J Kessler

Physikalisches Institut, Universität Münster, Wilhelm-Klemm-Strasse 10, D-48149 Münster, Federal Republic of Germany

Received 13 April 1994, in final form 4 July 1994

Abstract. Absolute differential cross sections (DCS) for elastic electron scattering and for electron impact excitation of xenon to the states $6s[\frac{3}{2}]_{1,2}$ were measured with the static-gas-target technique. In the energy range from 40 to 100 eV (elastic) and from 15 to 100 eV (inelastic) angles were varied from 3° (elastic) and 6° (inelastic) to 135°. The integral cross section for elastic scattering was calculated by subjecting the differential cross sections to a phaseshift analysis. A representation of the inelastic DCS in terms of the generalized oscillator strength was used to determine the optical oscillator strength of the excitation to the state $6s[\frac{3}{2}]_2$ and the integral electron impact excitation cross section. Our data were compared with recent theoretical results.

1. Introduction

Although electron–atom collisions have been studied for several decades, reliable absolute measurements of electron impact excitation cross sections for heavy elements at low energies are still rare. The difficulty of absolute measurements results mainly from the fact that they require accurate knowledge of the absolute target density, the geometry of the experimental arrangement, and the incident and scattered currents.

It is the main purpose of this paper to present absolute differential cross sections for electron impact excitation of xenon from the ground state $5p^6\ ^1S_0$ to the first excited states $6s[\frac{3}{2}]_{1,2}$ (cf figure 1). The measurements were motivated by several reasons. First, there are significant discrepancies between the few experiments done so far (Filipovic *et al* 1988, Suzuki *et al* 1991, Nishimura *et al* 1992). Besides, these experimental results do not agree with theoretical predictions by Bartschat and Madison (1987) and Zuo *et al* (1992). Furthermore, the experiment can be seen in the broader context of complete or 'perfect' experiments, which measure the complete set of observables by which a collision process is determined: electron collisions with heavy atoms are described by more than one scattering amplitude (Mott and Massey 1965, Kessler 1985, Bartschat and Madison 1988), so that one has to measure several independent observables in order to obtain a complete picture of the process under study. It turns out that it is not the polarization parameters, but the cross sections that are the weakest point in the complete experiments which have been made so far (Berger and Kessler 1986, Kessler 1986). The present experiment is a first step towards a complete inelastic experiment in which also the polarization parameters are to be determined.

0953-4075/94/184295+14$19.50

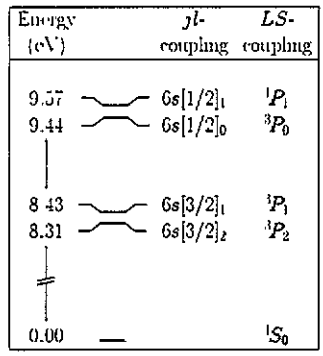

Figure 1. Diagram of the relevant energy levels of xenon. Excitation of $6s[\frac{3}{2}]_{1,2}$ has been studied.

Contrary to the results of the other groups, the data presented have been measured using a static gas target. As discussed in a previous paper (Peitzmann and Kessler 1990b) the static-gas method compared favourably in our laboratory with the method using crossed beams. Before the inelastic cross section measurements were started, measurements of elastic differential cross sections for electron scattering from xenon at 40, 60, 80 and 100 eV were performed. In addition to yielding new data they served to test the reliability of the apparatus and to get information on the systematic error limits of our cross section measurements. In contrast to the above-mentioned inelastic data, our absolute inelastic cross sections were not obtained by normalization to the elastic cross sections, but were absolutely measured *ab initio*. Reasonable error limits of such measurements were granted only when the electrons were not decelerated after the inelastic process. As a consequence, the resolution of the energy analyser was not sufficient to separate the excited states $6s[\frac{3}{2}]_{1,2}$ from each other, while they were separated from the other states shown in figure 1. The measurements were performed at incident energies of 15, 30, 40, 80 and 100 eV. An extrapolation procedure based on Lassettre *et al* (1969) makes it possible to determine the optical oscillator strength and the integral impact-excitation cross section.

2. Experimental procedure

2.1. Method

The technique of measuring absolute differential cross sections $\sigma(\theta)$ with a static gas target was described in detail by Bromberg (1969) and Holtkamp *et al* (1987). Therefore, only a brief discussion will be given here. The primary electron beam passes through a scattering cell which is completely filled with xenon gas. At a certain angle θ an analyser selects all electrons which have the energy desired. In the case of single scattering the scattered current I_s is given by

$$I_s = I_0 n \sigma(\theta) l \, d\Omega \tag{1}$$

where I_0 is the primary current, n the number density of the target and $l\,d\Omega$ the product of scattering path length and solid angle subtended by the analyser. In order to determine $\sigma(\theta)$ absolutely the ratio I_s/I_0 and the quantity n (via pressure and temperature measurements) have to be measured. The quantity $l\,d\Omega$ takes into account that the detected electrons have been scattered into a finite volume. It can be calculated from

the geometry of the aperture system, the primary beam, and the angular distribution of the differential cross section $\sigma(\theta)$ (Critchfield and Dodder 1949). In our experiment the aperture system consists of a vertical front slit followed by the circular entrance hole of the analyser.

In a real experiment equation (1) needs, however, some further modification for describing the measurable current I_s' correctly. Both the primary and the scattered beam are attenuated on their paths through the target gas so that the scattered current I_s will be underestimated. In order to take this into account one has, for each scattering angle, to extrapolate linearly the expression $\ln(I_s' n_0/I_0 n)$ versus n to zero target density (n_0, i.e. one atom per unit volume is introduced to make the expression dimensionless). The intersection with the ordinate yields the desired value of $\sigma(\theta)$ given in equation (1). But this attenuation is not the only process which affects the measured current I_s'. Plural scattering, mainly double scattering (successive scattering by θ_1 and θ_2 with $\theta_1 + \theta_2 = \theta$), leads to an overestimation of I_s. As pointed out by Holtkamp *et al* (1987) this results in the pressure range used (1.2×10^{-2}–1.2×10^{-1} Pa) in different slopes of the plots which may change even in sign, but the value of $\sigma(\theta)$ at $n=0$ is not affected. An example is given in figure 2 for 80 eV where attenuation dominates at 25°, 35° and 40° (negative slopes) whereas plural scattering changes the slope to a positive sign at 30°.

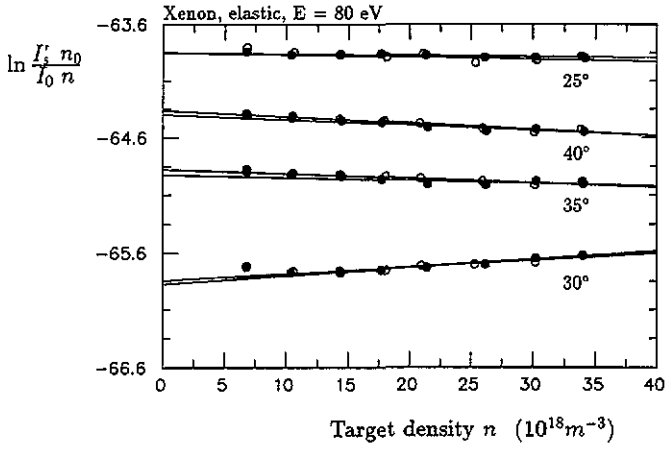

Figure 2. Extrapolation of $\ln(I_s' n_0/I_0 n)$ versus the target density n for 80 eV. The two straight lines for each scattering angle refer to symmetric scattering to the right (●) and to the left (○). The slopes of the lines change due to plural scattering (see text).

In order to determine $\sigma(\theta)$ absolutely it is not necessary to measure the currents I_s and I_0 absolutely, but they have to be measured with the same efficiency, i.e. with Faraday cups of the same geometry and with electrometers which, at different ranges, are cross-checked for internal consistency. This set-up could only be used at the scattering angles given in table 1 where the cross sections were sufficiently large. Measurements over the whole angular range were made with a channeltron as a detection device for the scattered current. This yields only relative values of $\sigma(\theta)$ because of the unknown efficiency of the channeltron. But in the range of overlap with the absolutely measured cross sections at small angles, the currents measured with the channeltron can be normalized.

2.2. Apparatus

Many parts of the apparatus need not be described here in detail because they were presented before by Holtkamp *et al* (1987). A perspective drawing of the scattering cell

Table 1. The scattering angles where the absolute DCS were directly measured without any normalization procedure.

Energy (eV)	Elastic	$6s[\frac{3}{2}]_{1,2}$
100	3°–50°	6°, 8°
80	5°–55°	6°–10°
60	5°–25° 110°–130°	—
40	5°–35° 100°–130°	6°–12°
30	—	6°–12°
15	—	6°, 8°

is given in figure 3. A vacuum chamber includes the scattering cell, which consists of a rotating top (containing the electron source) and a fixed bottom (containing the analyser and the opening for the gas inlet). The background pressure within the chamber was between 2×10^{-5} Pa and 6×10^{-4} Pa and the xenon pressure within the scattering cell itself was varied between 1.2×10^{-2} Pa and 1.2×10^{-1} Pa (measured with a spinning rotor gauge). The xenon pressure was adjusted with a computer-controlled variable leak valve. The Earth's magnetic field was reduced to less than 0.8 A m^{-1}.

We used two different electron sources. For the measurement of the elastic DCS a non-monochromatic electron beam ($\leqslant2\times10^{-6}$ A at 100 eV) was produced by a source described by Holtkamp *et al* (1987). For the inelastic experiment the monochromator consisting of two semi-hemispherical spectrometers (Jost 1979a, b) used by Peitzmann and Kessler (1990a) was improved. In order to increase the intensity, an electron optical lens system designed by Erdmann and Zipf (1982) was inserted to focus the electrons

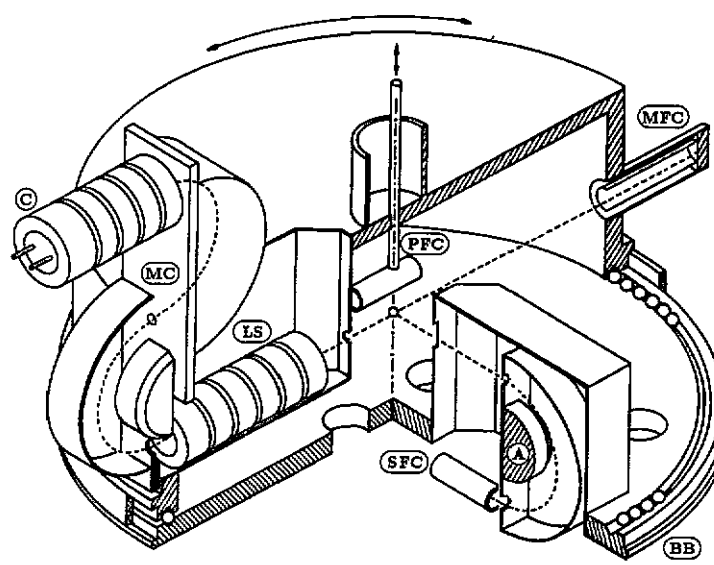

Figure 3. Perspective view of the scattering cell used for the inelastic measurements: C, cathode; MC, monochromator; LS, electrostatic lens system; PFC, Faraday cup for the primary electrons; MFC, monitoring Faraday cups; A, analyser; SFC, Faraday cup for the scattered electrons; BB, ball bearing.

emerging from the hairpin cathode on the entrance hole of the monochromator. With this arrangement a primary current of $\leqslant 2.2 \times 10^{-7}$ A (at 100 eV) with typically 210 meV FWHM was available. The angular divergence, i.e. the angle at which the intensity of the electron beam drops to half maximum, was estimated using a luminescent screen (elastic measurement) or—with the lower primary currents of the inelastic measurement—using two concentric Faraday cups. In the elastic case we obtained a parallel beam of typically 1 mm diameter. The angular divergence (FWHM) of the monochromatic beam was between 1.5° at 100 eV and 2.2° at 15 eV.

The energy scale was calibrated in the elastic measurement with an uncertainty of ±250 meV using the electron-impact excitation function of the optical transition $7p[\frac{5}{2}]_3 \rightarrow 6s[\frac{3}{2}]_2$ (467 nm). In order to calibrate the energy of the monochromatic electron beam, the $5p^5 6s^2\ ^2P_{3/2}$ resonance of xenon at 7.90 eV was observed. Figure 4 shows an example of the resonance. The uncertainty of the energy scale based on this calibration was about ±80 meV.

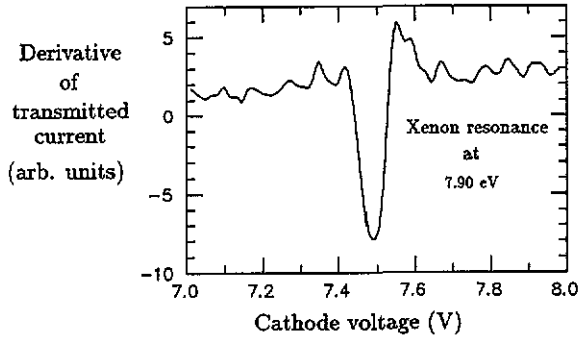

Figure 4. The $5p^5 6s^2\ ^2P_{3/2}$ resonance of xenon: the derivative of the transmitted current which was measured in the monitoring Faraday cups plotted against cathode voltage.

By an appropriate choice of the entrance and exit apertures of the analyser, as described by Holtkamp *et al* (1987), it was warranted that all electrons of the selected energy that had passed the entrance hole reached the detector. The total angular resolution, as given by the primary beam spread and the angular acceptance of the analyser, was between 1.2° and 1.5° and between 2.5° and 3.5° (FWHM) for the elastic and inelastic DCS, respectively.

For the direct measurement of the absolute DCS it is necessary to have Faraday cups with equal efficiencies to measure the primary and the scattered current. In a series of auxiliary measurements we found that the efficiency becomes independent of the intensity, divergence and energy of the detected beam if the Faraday cups have the same geometry and are equipped with an insulated entrance aperture with a negative potential (e.g. at −40 V for 100 eV electrons) against the grounded cups.

3. Error analysis

Each of the parameters in equation (1) is subject to several experimental uncertainties which depend on the special experimental situation. Most of them and the way to cope with them have been discussed by Holtkamp *et al* (1987) and Peitzmann and Kessler (1990a). For the present experiment we have improved details of the apparatus to reduce the uncertainties.

The pressure measurement was done with a spinning rotor gauge that has been recalibrated at the Physikalisch-Technische Bundesanstalt. The total systematic uncertainty in the target-density measurement amounts to about $\Delta_n = 2\%$.

The uncertainty Δ_I of the current measurements is between 1.7% (at 100 eV) and 2.7% (at 40 eV) for the measurement of the elastic DCS. Near the minima of the elastic DCS the scattering signal caused by residual gas molecules measured without xenon was subtracted. The uncertainty Δ_r due to the residual gas depends strongly on the scattering angle, is mostly negligible, and is 10% in the worst case (at 60 eV and 15°). Since in the inelastic experiment the scattered currents were lower we obtained larger uncertainties Δ_I. They ranged from 3.7% at 100 eV to 5.5% at 15 eV. Owing to computer-controlled operation of the electrometers used for the current measurements, the influence of the electrometer fluctuations mentioned by Peitzmann and Kessler (1990a) could be eliminated. Uncertainties of the primary-current measurements depending on the position of the Faraday cup, as described by Holtkamp *et al* (1987), were minimized by using a Faraday cup with negative entrance aperture (cf section 2.2).

The scattering path length has an uncertainty Δ_{path} of <2.5% if an idealized primary beam of zero diameter is assumed. The correction—calculated using formulae derived by Critchfield and Dodder (1949)—for the real beam geometry is <1% at angles below 10° in the elastic experiment and between 3% and 5% below 15° for the inelastic DCS. At larger angles this correction is much smaller. The values given in tables 2 and 3 are corrected for this systematic error. The uncertainty of the differential cross section is enhanced by the magnitude of this real beam correction, because the density distribution of the primary electron beam in the experiment differs from that assumed by Critchfield and Dodder (1949). It was estimated from the geometry of the exit apertures of the electron source and—for the inelastic experiment—from current measurements using two concentric Faraday cups (MFC in figure 3). The influence of the finite angular resolution is included by this correction.

The uncertainty Δ_{fit} caused by fitting the relative data to the absolute DCS (least-squares fit) is between 3% and 4% and between 9% and 14% for the elastic and inelastic measurements, respectively.

The total error Δ given in tables 2 and 3 was computed for each value of $\sigma(\theta, E)$ individually by adding the contributions quadratically, i.e. assuming that they are uncorrelated,

$$\Delta^2 = \Delta_{stat}^2 + \Delta_n^2 + \Delta_I^2 + \Delta_r^2 + \Delta_{path}^2 + \Delta_{fit}^2 \tag{2}$$

where Δ_{stat} is the statistical error obtained by the extrapolation to zero target density (cf section 2.1). The other terms are the aforementioned contributions. Typical total uncertainties of the elastic DCS are between 4.5% at 100 eV and 6% at 40 eV. For the electron impact excitation DCS the typical uncertainty increases, e.g. to 15% at 15 eV.

4. Results

4.1. Cross sections for elastic scattering

4.1.1. Differential cross sections for elastic scattering. The measured elastic differential cross sections are listed in table 2. For 100 eV and 40 eV they are additionally presented in figure 5. The comparison with experimental results given by Holtkamp (1981), Register *et al* (1986), and Nishimura *et al* (1987), all of whom used the atomic beam

Table 2. Absolute differential cross sections and absolute uncertainties in units of $a_0^2\,sr^{-1}$ for elastic electron xenon scattering. The integral elastic cross section Q_{int} and the momentum transfer cross section Q_{mom} in units of $a_0^2\,sr^{-1}$ are given in the last two rows.

	100 eV		80 eV		60 eV		40 eV	
θ (deg)	$\sigma_{cls}(\theta)$	$\Delta(\theta)$	$\sigma_{cls}(\theta)$	$\Delta(\theta)$	$\sigma_{cls}(\theta)$	$\Delta(\theta)$	$\sigma_{cls}(\theta)$	$\Delta(\theta)$
3	142.7	6.2						
4	122.5	5.1						
5	103.6	4.5	113.4	4.5	120.8	4.9	118.8	5.4
6	87.0	3.6						
7	72.9	2.8						
8	60.6	2.4						
9	50.8	2.2						
10	41.7	1.6	47.4	2.1	56.3	2.4	65.0	2.9
11	34.4	1.3						
12	28.4	1.1						
15	14.07	0.52	18.17	0.73	23.8	1.0	33.6	1.4
20	3.60	0.17	5.39	0.28	8.42	0.37	17.00	0.72
25	0.589	0.050	1.018	0.060	2.45	0.10	8.08	0.33
30	0.419	0.026	0.149	0.015	0.469	0.039	3.81	0.17
35	0.989	0.056	0.476	0.018	0.145	0.016	1.806	0.087
40	1.390	0.047	0.890	0.033	0.221	0.018	0.843	0.052
45	1.355	0.050	1.017	0.039	0.290	0.017	0.335	0.026
50	0.977	0.056	0.833	0.032	0.241	0.014	0.166	0.016
55	0.558	0.026	0.506	0.025	0.1490	0.0090	0.194	0.014
60	0.189	0.011	0.222	0.011	0.0632	0.0052	0.313	0.018
65	0.0331	0.0022	0.0489	0.0046	0.0287	0.0031	0.441	0.024
70	0.0807	0.0040	0.0257	0.0026	0.0284	0.0031	0.482	0.029
75	0.261	0.012	0.0944	0.0060	0.0346	0.0026	0.459	0.027
80	0.453	0.021	0.1790	0.0088	0.0259	0.0022	0.390	0.021
85	0.571	0.025	0.224	0.010	0.0089	0.0015	0.336	0.018
90	0.562	0.024	0.2156	0.0098	0.0158	0.0020	0.381	0.022
95	0.464	0.022	0.1863	0.0084	0.0920	0.0083	0.541	0.033
100	0.312	0.015	0.1811	0.0086	0.261	0.018	0.837	0.049
105	0.199	0.010	0.239	0.012	0.522	0.034	1.212	0.072
110	0.1518	0.0067	0.359	0.018	0.771	0.056	1.529	0.093
115	0.1715	0.0084	0.504	0.024	1.012	0.060	1.74	0.11
120	0.216	0.011	0.599	0.027	1.135	0.065	1.73	0.10
125	0.237	0.010	0.600	0.027	1.086	0.064	1.456	0.084
130	0.1988	0.0089	0.479	0.023	0.857	0.061	1.026	0.068
135	0.1098	0.0095	0.280	0.018	0.530	0.041	0.496	0.040
Q_{int}	19.6	1.9	20.0	2.1	22.6	2.1	34.4	2.5
Q_{mom}	8.3	2.4	7.7	2.6	8.9	2.0	16.7	2.0

method, yields remarkably good agreement at all energies. Only the values given by Holtkamp (1981) at 60 eV between 60° and 90° are much too small because his apparatus was not appropriate for measuring such very low cross sections. The earlier cross sections by Williams and Crowe (1975) which are not shown in the figure differ substantially from our results at 60 eV.

The theoretical curves are fully relativistic calculations by Bartschat (1992), which are based on the work of Hasenburg *et al* (1986), and by McEachran and Stauffer (1987, 1992). Only the calculation by Bartschat includes an absorption potential, which results in lower values and thus in better agreement with the present data. In the angular

Table 3. Absolute differential cross sections $\sigma_{1,2}(\theta)$ and their absolute uncertainties in units of $a_0^2\,\mathrm{sr}^{-1}$ for the excitation of xenon $6s[\frac{3}{2}]_{1,2}$ by electron impact. The values in brackets [ ] are the negative exponents of an additional factor 10, e.g. at $E=100$ eV and $\theta=15°$ the cross section is $(0.142\pm0.019)\,a_0^2\,\mathrm{sr}^{-1}$. The integral cross sections $Q_{1,2}$ for the $6s[\frac{3}{2}]_{1,2}$ excitation are given in the last row.

	100 eV			80 eV			40 eV			30 eV			15 eV		
θ (deg)	$\sigma_{1,2}(\theta)$	$\Delta(\theta)$		$\sigma_{1,2}(\theta)$	$\Delta(\theta)$		$\sigma_{1,2}(\theta)$	$\Delta(\theta)$		$\sigma_{1,2}(\theta)$	$\Delta(\theta)$		$\sigma_{1,2}(\theta)$	$\Delta(\theta)$	
6	8.11	0.75	[0]	9.68	0.70	[0]	8.55	0.65	[0]	5.74	0.61	[0]	7.37	0.74	[1]
8	3.01	0.33	[0]	4.38	0.29	[0]	5.30	0.38	[0]	4.12	0.40	[0]	6.70	0.56	[1]
10	1.15	0.24	[0]	1.89	0.15	[0]	3.26	0.28	[0]	2.78	0.26	[0]	6.21	0.47	[1]
12							2.01	0.14	[0]	1.90	0.20	[0]			
15	1.42	0.19	[1]	2.63	0.25	[1]	8.92	0.87	[1]	1.14	0.14	[0]	4.27	0.65	[1]
20	6.63	0.85	[2]	8.43	0.81	[2]	2.82	0.27	[1]	5.31	0.64	[1]	2.81	0.43	[1]
25	3.96	0.50	[2]	5.47	0.52	[2]	1.30	0.12	[1]	3.05	0.37	[1]	1.95	0.30	[1]
30	1.70	0.22	[2]	2.81	0.27	[2]	8.89	0.86	[2]	2.08	0.25	[1]	1.71	0.26	[1]
35	7.42	0.95	[3]	1.12	0.10	[2]	6.39	0.62	[2]	1.42	0.17	[1]	1.65	0.25	[1]
40	6.43	0.83	[3]	5.81	0.57	[3]	4.46	0.45	[2]	1.00	0.12	[1]	1.61	0.25	[1]
45	7.22	0.93	[3]	5.04	0.50	[3]	3.07	0.32	[2]	7.24	0.87	[2]	1.58	0.24	[1]
50	6.74	0.86	[3]	5.27	0.57	[3]	2.01	0.20	[2]	5.29	0.64	[2]	1.49	0.23	[1]
55	5.02	0.66	[3]	4.47	0.46	[3]	1.37	0.13	[2]	4.24	0.51	[2]	1.39	0.21	[1]
60	2.67	0.36	[3]	3.14	0.32	[3]	9.54	0.93	[3]	3.44	0.41	[2]	1.24	0.19	[1]
65	1.18	0.16	[3]	1.52	0.22	[3]	6.95	0.67	[3]	2.58	0.32	[2]	1.11	0.17	[1]
70	7.8	1.1	[4]	8.5	1.6	[4]	5.40	0.53	[3]	1.99	0.24	[2]	9.83	1.5	[2]
75	1.30	0.17	[3]	7.4	1.2	[4]	4.68	0.52	[3]	1.68	0.20	[2]	8.69	1.3	[2]
80	2.36	0.31	[3]	1.13	0.16	[3]	4.37	0.43	[3]	1.56	0.19	[2]	7.93	1.2	[2]
85	3.08	0.39	[3]	1.25	0.26	[3]	4.54	0.47	[3]	1.65	0.20	[2]	6.22	0.94	[2]
90	3.09	0.41	[3]	9.1	1.1	[4]	5.88	0.60	[3]	1.74	0.20	[2]	5.60	0.86	[2]
95	2.67	0.36	[3]	8.7	2.0	[4]	6.69	0.69	[3]	1.77	0.21	[2]	5.60	0.84	[2]
100	1.95	0.25	[3]	1.00	0.13	[3]	8.40	0.81	[3]	1.68	0.20	[2]	5.12	0.77	[2]
105	1.43	0.23	[3]	1.46	0.22	[3]	1.01	0.10	[2]	1.47	0.18	[2]	5.23	0.80	[2]
110	1.30	0.17	[3]	2.10	0.24	[3]	1.10	0.12	[2]	1.25	0.15	[2]	6.22	0.94	[2]
115	1.47	0.21	[3]	3.10	0.30	[3]	1.18	0.12	[2]	1.02	0.13	[2]	7.0	1.1	[2]
120	1.73	0.22	[3]	3.69	0.37	[3]	1.12	0.11	[2]	9.4	1.2	[3]	7.0	1.0	[2]
125	1.69	0.21	[3]	3.85	0.40	[3]	9.62	0.93	[3]	9.8	1.3	[3]	7.2	1.1	[2]
130	1.58	0.26	[3]	3.16	0.30	[3]	8.33	0.81	[3]	1.11	0.14	[2]	7.9	1.2	[2]
135	1.21	0.29	[3]	2.12	0.21	[3]	6.31	0.62	[3]	1.32	0.16	[2]	8.5	1.3	[2]
$Q_{1,2}$	1.23	0.25	[0]	1.26	0.20	[0]	1.24	0.15	[0]	1.26	0.17	[0]	1.54	0.37	[0]

range up to 30° at 100, 80 and 60 eV the results of both calculations agree with our measurement.

The absolute elastic cross section is one of the fundamental observables that are required for the evaluation of the magnitudes and phases of the complex amplitudes f and g describing spin-dependent elastic electron scattering ('complete' experiment). Such an evaluation has been done by Berger and Kessler (1986) using polarization parameters measured in our laboratory and cross sections from various groups. We have used the present elastic cross sections and some more recent polarization data for a re-evaluation of f and g, so that the experimental values for these complex amplitudes are now based on data from one and the same laboratory. It turned out that, within the experimental error limits, this did not significantly change the previously published data of Berger and Kessler (1986), as far as they are based on cross sections of Register *et al* (1986) and Holtkamp (1981).

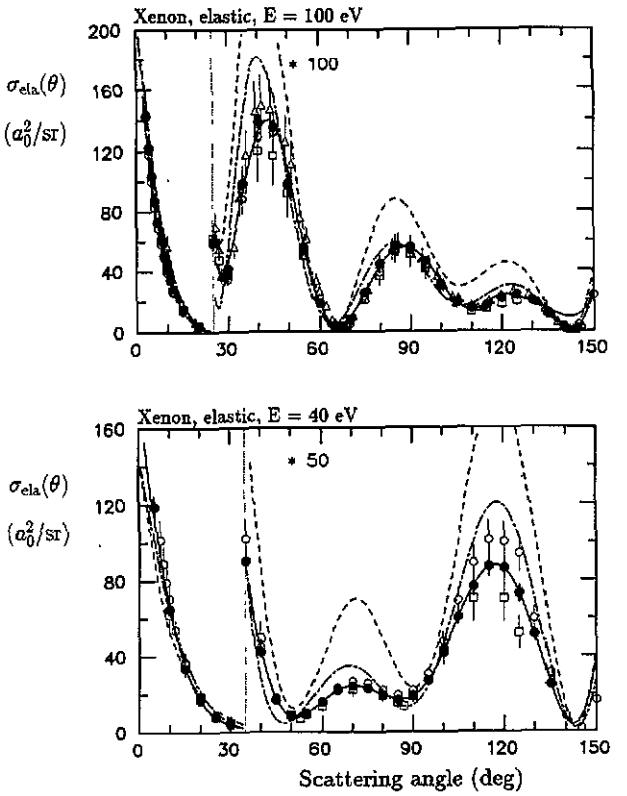

Figure 5. Absolute differential cross sections for elastic electron–xenon scattering at 100 and 40 eV; ●, this work; ○, Holtkamp (1981); □, Nishimura *et al* (1987); △, Register *et al* (1986); — — —, Bartschat (1992); ——, McEachran and Stauffer (1987, 1992); ——, phaseshift analysis (based on equation (6)).

4.1.2. Integral cross sections for elastic scattering. In order to evaluate the integral elastic cross section

$$Q_{ela} = 2\pi \int_0^{\pi} \sigma_{ela}(\theta) \sin\theta \, d\theta \tag{3}$$

the measured DCS have to be extrapolated to 0° and 180°. This can be achieved by using a suitable parametrization of the angular distribution

$$\sigma_{ela} = |f(\theta)|^2 \tag{4}$$

where $f(\theta)$ is expressed in terms of real phaseshifts η_l (Register *et al* 1980, Nishimura *et al* 1987)

$$f(\theta) = \frac{1}{2ik_1} \sum_{l=0}^{\infty} (2l+1)(e^{2i\eta_l} - 1) P_l(\cos\theta). \tag{5}$$

Here k_1 is the electron wavenumber and P_l are the Legendre polynomials. The contribution of the higher partial wave can, according to Thompson (1966), be taken into

account by the approximate relation

$$f(\theta)=\frac{1}{2ik_1}\sum_{l=0}^{L}(2l+1)(e^{2i\eta_l}-1)P_l(\cos\theta)+f_B^L(\theta) \tag{6}$$

with

$$f_B^L(\theta)=\pi\alpha k_1\left[\tfrac{1}{3}-\tfrac{1}{2}\sin\tfrac{1}{2}\theta-\sum_{l=1}^{L}\frac{P_l(\cos\theta)}{(2l+3)(2l-1)}\right] \tag{7}$$

where $\alpha=27.3\ a_0^3$ is the atomic polarizability of xenon. In order to obtain a set of $L+1$ phases we have minimized the expression

$$\chi^2=\frac{1}{N-L-1}\sum_{i=1}^{N}\left[\frac{\sigma_{ela}(\theta_i)-\sigma_{fit}(\theta_i)}{\Delta(\theta_i)}\right]^2 \tag{8}$$

using N measured cross sections $\sigma_{ela}(\theta_i)$ and their uncertainties $\Delta(\theta_i)$. $\sigma_{fit}(\theta_i)$ is the cross section calculated with equations (4) and (6). The angular distributions thus obtained are shown by the full lines in figure 5, where 12 and 10 phases were varied resulting in $\chi^2=2.14$ and $\chi^2=0.20$ at 100 eV and 40 eV, respectively. These curves are reasonable extrapolations to angles not covered by the experiment. The values of the

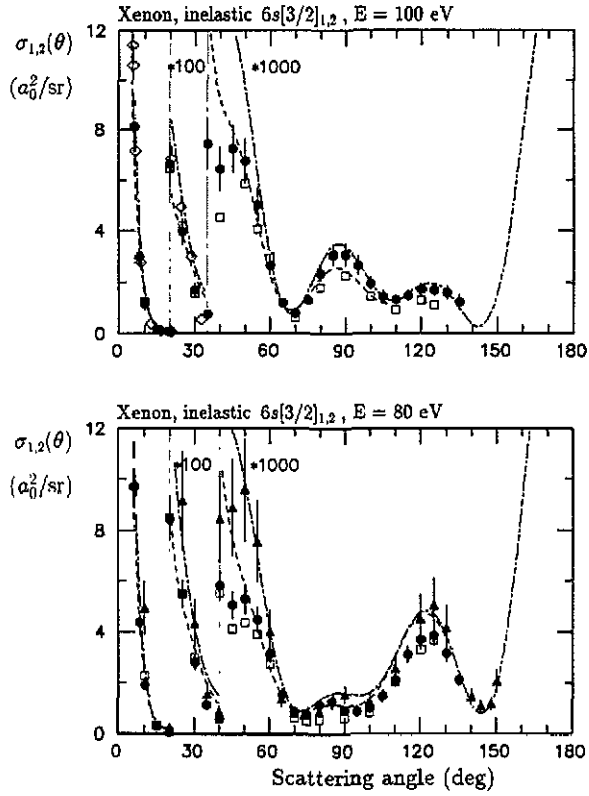

Figure 6. Absolute differential cross sections for the excitation of xenon $6s[\frac{3}{2}]_{1,2}$ by electron impact at 100, 80, 40, 30 and 15 eV; ●, this work; □, Nishimura *et al* (1985, 1992); ▲, Filipovic *et al* (1988); — - —, Bartschat (1992); -----, Zuo *et al* (1992).

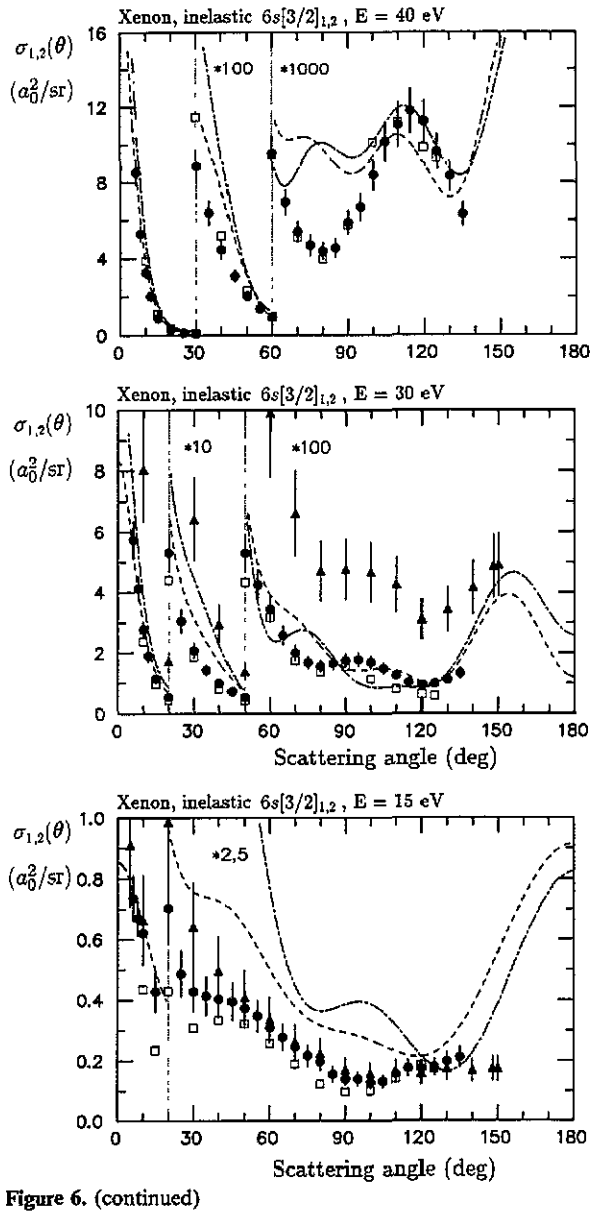

Figure 6. (continued)

integral elastic cross section Q_{ela} and the momentum transfer cross section

$$Q_{mom} = 2\pi \int_0^{\pi} (1 - \cos\theta)\sigma_{ela}(\theta) \sin\theta \, d\theta \tag{9}$$

are also given in table 2. The uncertainty of these values caused by the uncertainty of the extrapolated contribution to the integral was estimated by varying the upper index L in equation (6) which yielded different results for χ^2 in equation (8). Considering the factor $(1 - \cos\theta)$ in equation (9) the contribution of the extrapolated angular range to the momentum transfer cross section Q_{mom} is between 62% and 44% at 100 eV and 40 eV, respectively.

4.2. Cross sections for electron impact excitation

4.2.1. Differential cross sections for electron impact excitation. The DCS $\sigma_{1,2}(\theta)$ for electron impact excitation of the (unresolved) states $6s[\frac{3}{2}]_1$ and $6s[\frac{3}{2}]_2$ are listed in table 3. Figure 6 shows these values in comparison with results of other authors. At those angles and energies ($E \leqslant 40$ eV) where these authors measured the cross sections for excitation of the states $6s[\frac{3}{2}]_1$ and $6s[\frac{3}{2}]_2$ separately, we show the sum of their data.

At 100 eV our results agree with those of Suzuki *et al* (1991) at scattering angles below 30°. They also agree at this and at the other energies and for most of the angles with the preliminary data of Nishimura *et al* (1985, 1992) for which, unfortunately, error bars have not been given. The cross sections given by Filipovic *et al* (1988) differ from our values at 80 eV at angles below 60° and at 30 eV over the whole angular range. Suzuki *et al* (1991) also found that the cross sections of Filipovic *et al* (1988) at 80 eV are too large. At 15 eV all experimental values agree within the error limits if we assume realistic uncertainties of the data measured by Nishimura *et al* (1985, 1992).

The theoretical curves shown in figure 6 are distorted-wave Born approximation (DWBA) calculations of Bartschat and Madison (1987) and of Zuo *et al* (1992). At 100 and 80 eV both calculations reproduce the shape and the size of the present curves except in the angular range around 40° where the theoretical curves do not show the slight experimental minimum. At 40, 30 and 15 eV the theoretical calculations predict a different shape for scattering angles larger than 50°, giving e.g. at 40 eV two minima in contrast to the single measured minimum at 80°. The experimental and theoretical data agree, however, at low angles, the results of Zuo *et al* (1992) coming closer to the experimental values than the data of Bartschat and Madison (1987).

4.2.2. Generalized oscillator strengths. The representation of the DCS in terms of generalized oscillator strengths (GOS) enables one to check the range of validity of the first Born approximation, to derive the optical oscillator strength (OOS), and to calculate the integral cross section. The generalized oscillator strengths F and the differential cross sections $\sigma_{1,2}$ are related by

$$F=\frac{W}{4R_0}\frac{k_1}{k_2}(Ka_0)^2\frac{\sigma_{1,2}}{a_0^2}. \tag{10}$$

Here $W=8.43$ eV is the excitation energy of the state $6s[\frac{3}{2}]_1$, $\hbar k_1$ and $\hbar k_2$ are the electron momenta before and after scattering, $\hbar K=|\hbar k_1-\hbar k_2|$ is the momentum transfer caused by the excitation of the state $6s[\frac{3}{2}]_1$, and R_0 is the Rydberg energy. Equation (10) holds only approximately for the situation investigated here, since excitation energy and momentum transfer for $6s[\frac{3}{2}]_2$ differ slightly from those for $6s[\frac{3}{2}]_1$. The errors caused by this approximation were calculated using Nishimura's (1992) DCS for separate excitation of the two levels and were found to be smaller than 1% for $E \geqslant 30$ eV and 2% for $E=15$ eV. In figure 7 the GOS are plotted against K^2 showing that at energies $E \geqslant 80$ eV the first Born approximation is valid, because the GOS depend only on K^2 and not on the energy itself.

It has been shown by Lassettre *et al* (1969) that the extrapolations of $F(K)$ to zero momentum transfer yields the optical oscillator strength (OOS). Following Klump and Lassettre (1978) we use the expansion

$$F=\frac{1}{(1+x^2)^6}\left[F_0+\sum_{n=1}^{\infty}F_n\left(\frac{x^2}{1+x^2}\right)^n\right] \tag{11}$$

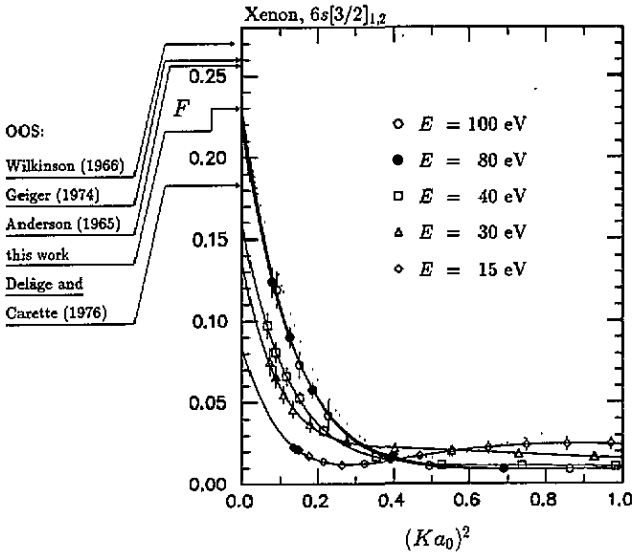

Figure 7. Generalized oscillator stength F for the $6s[\frac{3}{2}]_{1,2}$ excitation of xenon plotted against K^2 (square of momentum transfer) at incident energies between 100 and 15 eV. The dotted curve was found by Suzuki *et al* (1991) at 100 eV. The full curves were calculated using equation (11). The optical oscillator strengths (OOS) measured by different authors are marked at the ordinate.

where

$$x=\frac{K\alpha_0}{(V/R_0)^{1/2}+[(V-W)/R_0]^{1/2}}. \tag{12}$$

The coefficients F_0 and F_n, where F_0 is the optical oscillator strength, can be determined from the experimental data; V is the ionization potential. Using our experimental data we have evaluated the coefficients using a minimization procedure (least squares fit). For 100 eV, where we have seen that the Born approximation holds, we obtained $F_0=0.23\pm0.05$ in agreement with measurements by Anderson (1965), Wilkinson (1966), Geiger (1974) and Delâge and Carette (1976).

4.2.3. Integral cross sections for electron impact excitation. We have determined the integral cross section $Q_{1,2}$ for electron impact excitation of the states $6s[\frac{3}{2}]_{1,2}$ using the generalized oscillator strengths $F(K)$ and the relation (Vriens *et al* 1968)

$$Q_{1,2}=\frac{8\pi a_0^2R_0^2}{WE}\int_{K_{\min}a_0}^{K_{\max}a_0}\frac{F(K)}{Ka_0}\,\mathrm{d}(Ka_0) \tag{13}$$

with

$$K_{\min}=k_1-k_2 \qquad \text{and} \qquad K_{\max}=k_1+k_2.$$

The contribution of the small momentum transfers not covered by the measurement to the integral $Q_{1,2}$ was calculated with the fitting function (equation (11)). It amounts to values between 1% and 70% for energies between 15 eV and 100 eV, respectively. On the basis of the aforementioned uncertainty of the fit parameter F_0 the uncertainty of this contribution was set to 20%. For momentum transfers between the maximal values occurring in the experiment and the limit $K_{\max}$ we used the theoretical results of

Bartschat and Madison (1987) and Zuo *et al* (1992). The contribution of this large-angle range to $Q_{1,2}$ was between 25% at 15 eV and 0.6% at 100 eV. We made the conservative assumption that this contribution to $Q_{1,2}$ has an uncertainty of 50%. The error of $Q_{1,2}$ caused by the influence on the GOS of the small energetic difference of the two excited levels (cf section 4.2.2) was negligible compared to the other uncertainties.

The integral cross sections obtained by this procedure are also listed in table 3. They agree with the values given by Suzuki *et al* (1991) at 100 eV and by Filipovic *et al* (1988) at 15 eV. But there are large discrepancies with the data of Filipovic *et al* (1988) at 30 eV ($Q_{1,2}=(5.1\pm1.5)\,a_0^2$) and at 80 eV ($Q_{1,2}=(6.2\pm2.4)\,a_0^2$).

Acknowledgment

The authors wish to thank Professor K Bartschat, Professor A Stauffer and Professor H Nishimura for providing partly unpublished results.

References

Anderson D K 1965 *Phys. Rev.* **137** A21
Bartschat K 1992 Private communication, based on Hasenburg *et al* (1986)
Bartschat K and Madison D H 1987 *J. Phys. B: At. Mol. Phys.* **20** 5839
—— 1988 *J. Phys. B: At. Mol. Opt. Phys.* **21** 2621
Berger O and Kessler J 1986 *J. Phys. B: At. Mol. Phys.* **19** 3539
Bromberg J P 1969 *J. Chem. Phys.* **50** 3906
Critchfield C L and Dodder D C 1949 *Phys. Rev.* **75** 419
Delâge A and Carette J D 1976 *Phys. Rev.* A **14** 1345
Erdmann P W and Zipf E C 1982 *Rev. Sci. Instrum.* **53** 225
Filipovic D, Marinkovic B, Pejcev V and Vuskovic L 1988 *Phys. Rev.* A **37** 356
Geiger J 1974 *Proc. 4th Int. Conf. on Vacuum Ultraviolet Radiation Physics (Hamburg)* ed E E Koch, R Haensel and R Kunz (New York: Pergamon) Abstracts p 28
Hasenburg K H, Madison D H, Bartschat K and Blum K 1986 *J. Phys. B: At. Mol. Phys.* **19** 1803
Holtkamp G 1981 *Diploma thesis* University Münster
Holtkamp G, Jost, Peitzmann F J and Kessler J 1987 *J. Phys. B: At. Mol. Phys.* **20** 4543
Jost K 1979a *J. Phys. E: Sci. Instrum.* **12** 1001
—— 1979b *J. Phys. E: Sci. Instrum.* **12** 1006
Kessler J 1985 *Polarized Electrons* 2nd edn (Berlin: Springer)
—— 1986 *Comment. At. Mol. Phys.* **18** 279
Klump K N and Lassettre E N 1978 *J. Chem. Phys.* **68** 886
Lassettre E N, Skerbele A and Dillon M A 1969 *J. Chem. Phys.* **50** 1829
McEachran R P and Stauffer A D 1987 *J. Phys. B: At. Mol. Phys.* **20** 3483
—— 1992 Private communication
Mott N F and Massey H S W 1965 *The Theory of Atomic Collisions* 3rd edn (Oxford: Clarendon)
Nishimura H, Danjo A and Matsuda T 1985 *Proc. 14th Int. Conf. on the Physics of Electronic and Atomic Collisions (Palo Alto)* (Amsterdam: North-Holland) Abstracts p 108
—— 1992 Private communication
Nishimura H, Matsuda T and Danjo A 1987 *J. Phys. Soc. Jpn.* **56** 70
Peitzmann F J and Kessler J 1990a *J. Phys. B: At. Mol. Opt. Phys.* **23** 2629
—— 1990b *J. Phys. B: At. Mol. Opt. Phys.* **23** 4005
Register D F, Trajmar S and Srivastava S K 1980 *Phys. Rev.* **21** 1134
Register D F, Vuskovic L and Trajmar S 1986 *J. Phys. B: At. Mol. Phys.* **19** 1685
Suzuki T Y, Sakai Y, Min B S, Takayanagi T, Wakiya K and Suzuki H 1991 *Phys. Rev.* A **43** 5867
Thompson D G 1966 *Proc. R. Soc.* A **294** 160
Vriens L, Simpson J A and Mielczarek S R 1968 *Phys. Rev.* **165** 7
Wilkinson P G 1966 *J. Quant. Spectrosc. Radiat. Transfer* **6** 823
Williams J F and Crowe A 1975 *J. Phys. B: At. Mol. Phys.* **8** 2233
Zuo T, McEachran R P and Stauffer A D 1992 *J. Phys. B: At. Mol. Phys.* **25** 3393 and private communication